Instituto de Física
Universidade de São Paulo

Quasi free electrofission on ^{238}U

Likhachev[a], V.P.; Mesa, J.[a,b]; Arruda-Neto, J.D.T.[a,c]; Carlson, B.V.[d]; Deppman, A.[a], Hussein, M.S.[a]; Nesterenko, V.O.[e]; Garcia, F.[f] and Rodrigues, O[b]

[a] *Instituto de Física, Universidade de São Paulo, São Paulo, SP, Brazil*
[b] *Instituto Superior de Ciencias y Tecnologia Nucleares, Havana, Cuba*
[c] *Universidade de Santo Amaro, São Paulo, Brazil*
[d] *Instituto de Estudos Avançados - Centro Técnico Aeroespacial, São José dos Campos, Brazil*
[e] *Bogolubov Laboratory of Theoretical Physics, JINR, Dubna, Russia*
[f] *Universidade Estadual de Santa Cruz, Ilhéus, Bahia, Brazil*

Publicação IF - 1544/2002

UNIVERSIDADE DE SÃO PAULO
Instituto de Física
Cidade Universitária
Caixa Postal 66.318
05315-970 - São Paulo - Brasil

QUASI FREE ELECTROFISSION of ^{238}U.

V. P. Likhachev[a] J. Mesa[a,b] J. D. T. Arruda-Neto[a,c], B. V. Carlson[d], A. Deppman[a], M. S. Hussein[a], V. O. Nesterenko[e], F. Garcia[f] and O. Rodriguez[b].

[a] *Instituto de Física, Universidade de São Paulo, São Paulo, Brazil.*

[b] *Instituto Superior de Ciencias y Tecnologia Nucleares, Havana, Cuba.*

[c] *Universidade de Santo Amaro, São Paulo, Brazil.*

[d] *Instituto de Estudos Avançados-Centro Técnico Aeroespacial, São José dos Campos, Brazil.*

[e] *Bogolubov Laboratory of Theoretical Physics, JINR, Dubna, Russia.*

[f] *Universidade Estadual de Santa Cruz, Ilheus, Bahia, Brazil.*

Abstract

We present the result of a theoretical study of the quasi free electrofission of ^{238}U. The exclusive differential cross sections for the quasi free scattering reaction stage have been calculated in PWIA, using a Macroscopic-Microscopic approach for the description of the proton bound states. The nuclear shape was parametrized in terms of cassinian ovaloids. The equilibrium deformation parameters have been calculated by minimizing the total nuclear energy. In the calculation the axially deformed Woods-Saxon single particle potential was used. The obtained single particle momentum distributions were averaged over the nuclear symmetry axis direction. The occupation numbers were calculated in the BCS approach. The fissility for the single hole excited states of the residual nucleus ^{237}Pa was calculated on the statistical theory grounds both without taking into account the pre-equilibrium emission of the particle, and with preequilibrium emission in the framework of the exciton model.

I. INTRODUCTION

Quasi free scattering of high energy electrons (QF) on nuclei is the field of nuclear physics which is traditionally devoted to the study of the single particle aspects of nuclear structure: single particle binding energies, momentum distributions, occupation numbers, etc [1].

A new branch of these investigations is the study of decay channels of single hole states in the residual nucleus, created as a result of the QF process. Especially interesting is to study a fission decay following a QF process. In this case we have a single particle process in the first reaction stage, and essentially a collective process in the final reaction stage. The collective degrees of freedom are excited in the intermediate reaction stage due the residual interaction.

This is a new sort of nuclear reaction which may allow one to get unique information on the dissociation of well defined single hole configurations (which we can select by coincidence $(e, e'p)$) into complex nuclear configurations, and its role in nuclear fission. The new and most important aspect of this reaction is that, after knocking-out a proton, we obtain the heavy nucleus ^{237}Pa in a single hole doorway state (see discussion below) which could undergo nuclear fission. Indeed, instead of dealing with collective doorway states, which are coherent sums of a great number of 1p-1h configurations (as the well-known giant resonances), these non-collective doorway states will be represented by only one, well defined, 1h configuration. The residual interaction in ^{237}Pa mixes these 1h configurations into more complicate 2h-1p and 3h-2p ones. So, there would be some competing channels for fission. It may occur either directly from 1h configurations, or, with some delay, from mixed states (or their components). In a QF process we have in the initial state only one configuration; thus, the fission probability P_f should be more sensitive to the individual structure of this initial state as compared with conventional reactions, where the effects of the structure are averaged out over many single particle states forming the doorway.

The unambiguous extraction of single hole contributions is possible only in an exclu-

sive experimental scheme (reaction $(e, e'\ pf)$) and involves extremely thin targets (fission fragments have to leave the target with small energy losses), high energy resolution, and coincidence requirement between the final particles in order to separate the single hole states. The exclusive $(e, e'pf)$-experiment is very difficult for practical realization, and never has been so far performed. The integral contribution of the quasi free electron scattering to the fission process was studied only in inclusive experiments: (e, f) [2] and $(e, e'f))$ [3]. These works dealt only with the issue of the QF contribution in electrofission.

The advent of high energy, CW, electron accelerators combined with the development of high resolution facilities, opens the possibility of studying the fission channel for quasi free electron scattering in an exclusive experimental setup. The most suitable accelerator for this experiment is at the Thomas Jefferson National Accelerator Facility (TJNAF).

For excitation of the residual nucleus to an well defined single hole state, the initial and final state interactions have to be negligible. This situation corresponds to high momentum transfer and high proton exit energy, when the Plane Wave Impulse Approximation (PWIA) for the calculation of the quasi free electron scattering cross section is valid.

This work presents the results of a PWIA calculations for the quasi free $(e, e'p)$-differential cross section for deformed orbitals of ^{238}U, in the framework of the macroscopic-microscopic approach, plus an estimate of the fissility for single hole states in the residual nucleus ^{237}Pa, performed on the statistical theory grounds. These calculations could serve as first order magnitude guide-line for expected cross sections.

II. PWIA CROSS SECTION

In the first order Born approximation the electron with initial four-momentum $k_{1\mu} = (\vec{k}_1, i\varepsilon_1)$ and final $k_{2\mu} = (\vec{k}_2, i\varepsilon_2)$, transfers a virtual photon with four-momentum $q_\mu = (\vec{q}, i\omega) = k_{1\mu} - k_{2\mu}$, resulting in the final state a knocked-out nucleon with $p_\mu = (\vec{p_p}, iE_p)$ and a residual nucleus with $P_{A-1\mu} = (\vec{P}_{A-1}, iE_{A-1})$.

In the impulse approximation a virtual photon interacts with a bound nucleon (proton or neutron) of four-momentum $p_m = (\overrightarrow{p}_m, iE_m)$,which exits the nucleus with four-momentum $p_\mu = (\overrightarrow{p_p}, iE_p)$ without further interaction (no FSI). The corresponding momentum diagram in the impulse approximation is shown in Fig. 1 for the Laboratory system..

In the plane wave impulse approximation (PWIA) $\overrightarrow{p}_m = -\overrightarrow{P}_{A-1}$, and the missing quantities (momentum and energy of the proton before interaction) can be defined from the energy and momentum conservation law in the following way:

$$\overrightarrow{p}_m = \overrightarrow{p}_p - \overrightarrow{q}, \tag{1}$$

$$E_m = \omega - T_p - T_{A-1},$$

where $E_m = M_{A-1} + m_p - M_A$ is the proton missing (or separation) energy, T_p is the kinetic energy of the outgoing proton, and T_{A-1} is the kinetic energy of the residual nucleus. The momentum and energy transfer of the virtual photon can be varied independently.

In the PWIA the six folded differential cross section of the $(e, e'p)-$ reaction in the Laboratory system has the following form [4]:

$$\frac{d^6\sigma}{d\Omega_e\, d\Omega_p\, d\varepsilon_2 dE_p} = p_p E_p \sigma_{ep} S(E_m, \overrightarrow{p_m}), \tag{2}$$

where

$$\sigma_{ep} = \sigma_{mott}\left(V_C W_C + V_T W_T + V_I W_I + V_S W_S\right) \tag{3}$$

is the off-shell electron-nucleon cross section, $S(E_m, \overrightarrow{p_m})$ is the spectral function which defines the combined probability to find a bound proton with momentum $\overrightarrow{p_m}$ on the shell with separation energy E_m.

The kinematic functions V in Eq. (3) can be expressed , neglecting the mass of the electron, as:

$$V_C = \frac{q_\mu^4}{q^4}, \tag{4}$$

$$V_T = \frac{q_\mu^2}{2q^2} + \tan^2(\frac{\theta_e}{2}), \tag{5}$$

$$V_I = \frac{q_\mu^2}{q^2}\cos\phi\sqrt{\frac{q_\mu^2}{q^2}+\tan^2(\frac{\theta_e}{2})}, \tag{6}$$

$$V_S = \frac{q_\mu^2}{q^2}\cos^2\phi+\tan^2(\frac{\theta_e}{2}), \tag{7}$$

and

$$\sigma_{mott} = \frac{\alpha^2\cos^2\frac{\theta_e}{2}}{4\varepsilon_1^2\sin^4\frac{\theta_e}{2}}(1+\frac{2\varepsilon_1}{m_p}\sin^2\frac{\theta_e}{2})^{-1} \tag{8}$$

is the Mott cross section, ϕ is the angle between the scattering plane and the plane defined by the vectors $\overrightarrow{p}_p$ and $\overrightarrow{q}$.

For the structure functions W in Eq.(3) we use the off-shell prescription of de Forest [4]:

$$W_C = \frac{1}{4\bar{E}E_p}\{(\bar{E}+E_p)^2(F_1^2+\frac{\overline{q}_\mu^2}{4m_p^2}\kappa_p^2F_2^2)-q^2(F_1+\kappa_pF_2)^2\}, \tag{9}$$

$$W_T = \frac{\overline{q}_\mu^2}{2\bar{E}E_p}(F_1+\kappa_pF_2)^2,$$

$$W_I = -\frac{p_p\sin\gamma}{\bar{E}E_p}(\bar{E}+E_p)(F_1^2+\frac{\overline{q}_\mu^2}{4m_p^2}\kappa_p^2F_2^2),$$

$$W_S = \frac{p_p^2\sin^2\gamma}{\bar{E}E_p}(F_1^2+\frac{\overline{q}_\mu^2}{4m_p^2}\kappa_p^2F_2^2),$$

where κ_p =1.793 is the anomalous magnetic moment of the proton in units of the Bohr magneton ,

$$\bar{E} = \sqrt{p_m^2+m_p^2}, \tag{10}$$

m_p is the mass of the proton, $\overline{q}_\mu = (\overrightarrow{q}, i\overline{\omega})$, $\overline{\omega} = E_p - \overline{E}$, γ is the angle between $\overrightarrow{p}_p$ and $\overrightarrow{q}$,

F_1 and F_2 are the on-shell Dirac and Pauli proton form factors, respectively:

$$F_1(q_\mu^2) = \frac{1}{1+\frac{q_\mu^2}{4m_p^2}}[G_E(q_\mu^2)+\frac{q_\mu^2}{4m_p^2}G_M(q_\mu^2)], \tag{11}$$

$$\kappa_p F_2(q) = \frac{1}{1+\frac{q_\mu^2}{4m_p^2}}[G_M(q_\mu^2) - G_E(q_\mu^2)], \tag{12}$$

where

$$G_E(q_\mu^2) = (\frac{1}{1+\frac{q_\mu^2}{0.71}})^{-2}, \tag{13}$$

$$G_M(q_\mu^2) = \mu_p G_E(q_\mu^2)], \tag{14}$$

$\mu_p = 2.793$ is the proton magnetic moment in units of the Bohr magneton and q_μ^2 in Eq.(13) is in $(\mathrm{GeV/c})^2$.

In the independent particle shell model the spectral function for the spherical orbitals $\alpha \equiv nlj$ with binding energy E_α takes the simple form:

$$S(E_m, \overrightarrow{p_m}) = \delta\left(E - E_\alpha\right)\ \upsilon_\alpha^2\ n_\alpha\left(\overrightarrow{p_m}\right), \tag{15}$$

where υ_α^2 and $n_\alpha\left(p\right)$ are the occupation number and momentum distribution of the α orbital, respectively. The six folded $(e, e'p)-$cross section could be transformed into a five folded one:

$$\frac{d^5\sigma}{d\Omega_e\ d\Omega_p\ dE_p} = p_p E_p \sigma_{ep}\ \upsilon_\alpha^2 n_\alpha\left(\overrightarrow{p_m}\right), \tag{16}$$

where it is imposed energy and momentum conservation for the kinematics variables in σ_{ep}.

III. SINGLE PARTICLE BOUND STATES

The single particle bound state energies and momentum distributions were calculated in the framework of the macroscopic-microscopic approach by using the BARRIER code [5].

The energy of the nucleus is presented as:

$$E_{tot} = E_{LD} + \delta E_{shell}, \tag{17}$$

where E_{LD} is the macroscopic liquid drop part of the energy and δE_{shell} is the shell correction, which describes shell and pairing effects. Both shell correction and the macroscopic part of the energy have been calculated according to [5].

A. Nuclear shape parametrization

Only axially symmetric nuclear shapes have been considered in the present work, and the deformed shape (up to and beyond its separation into two fragments) can be conveniently described by the Cassini ovoids [6,7]. The potential-energy surfaces are calculated as functions of ε (elongation) and α_4 (hexadecapolar momentum). From these potential energy surfaces, the equilibrium (ground state) deformation parameters ε and α_4 were calculated by minimizing the total nuclear energy (Eq.(17)): $\varepsilon = 0.227$ and $\alpha_4 = 0.059$.

B. Nuclear Potential

An Woods- Saxon potential [8], consisting of the central part V, spin-orbit V_{SO}, and the Coulomb potential V_{Coul} for protons, was employed:

$$V^{WS}(r,z,\varepsilon,\widehat{\alpha}) = V(r,z,\varepsilon,\widehat{\alpha}) + V_{so}(r,z,\varepsilon,\widehat{\alpha}) + V_{Coul}(r,z,\varepsilon,\widehat{\alpha}) \tag{18}$$

The real potential $V(r,z,\varepsilon,\widehat{\alpha})$ involves the parameters V_0, r_0 and a , describing the depth of the central potential, the radius and the diffuseness parameter, respectively, and it is expressed as:

$$V(r,z,\varepsilon,\widehat{\alpha}) = \frac{V_0}{1 + exp\left[\frac{dist(r,z,\varepsilon,\widehat{\alpha})}{a}\right]}, \tag{19}$$

where $dist(r,z,\varepsilon,\widehat{\alpha})$ is the distance between a point and the nuclear surface, and ε and $\widehat{\alpha}$ are deformation parameters.

The depth of the central potential is parametrized as

$$V_0 = V_0[1 \pm \kappa(N-Z)/(N+Z)], \tag{20}$$

with the plus sign for protons and the minus sign for neutrons, with the constant $\kappa = 0.63$.

The spin-orbit interaction is then given by:

$$V_{so}(r,z,\varepsilon,\widehat{\alpha}) = \lambda\left(\frac{h}{2Mc}\right)^2 \nabla V(r,z,\varepsilon,\widehat{\alpha}) \cdot (\vec{\sigma} \times \vec{p}), \tag{21}$$

where λ denotes the strength of the spin–orbit potential and M is the nucleon mass. The vector operator $\vec{\sigma}$ stands for Pauli matrices and $\vec{p}$ is the linear momentum operator.

The Coulomb potential is assumed to be that corresponding to the nuclear charge $(Z-1)e$, taken to be uniformly distributed inside the nucleus. It is computed in cylindrical coordinates by using the expression given in [6].

C. Single particle potential parameter definitions

For the ground state deformation of ^{238}U, small changes in λ (spin-orbit potential strength) and r_{0-so} (spin-orbit potential radius) of the Chepurnov parameters [9] are introduced in order to reproduce adequately the spin/parity of the levels sequence. Using single particle states obtained by this procedure, the quasiparticle states can be calculated for the first minimum region, providing spin, parity, energy and level spacing for the ground and some low–lying states. The quasiparticle spectrum was obtained by using the semi-microscopic combined method [10].

The potential parameters were chosen to give the best fit to the spectrum of single-quasiparticle excitations of the Z-odd neighboring nuclei ^{239}Np.

D. Single particle wave functions

The Hamiltonian matrix elements are calculated with the wave functions of a deformed axially symmetric oscillator potential. The wave functions in the coordinate space ϕ_i are expanded into eigenfunctions of the axially deformed harmonic oscillator potential.

These eigenfunctions form a complete orthonormal basis for the single particle Woods-Saxon wave function

$$\Psi_i\left(\overrightarrow{R},\sigma\right)=\sum_{n_\rho,n_z,\Lambda,\Sigma} C^i_{n_\rho,n_z,\Lambda,\Sigma}\Phi_{n_\rho,n_z,\Lambda,\Sigma}\left(\overrightarrow{R},\sigma\right). \tag{22}$$

From this expansion, we may conveniently express the single particle Woods-Saxon wave function in momentum space:

$$\widetilde{\Psi}_i\left(\overrightarrow{K},\sigma\right)=\sum_{n_\rho,n_z,\Lambda,\Sigma}C^i_{n_\rho,n_z,\Lambda,\Sigma}\widetilde{\Phi}_{n_\rho,n_z,\Lambda,\Sigma}\left(\overrightarrow{K},\sigma\right), \tag{23}$$

with

$$\widetilde{\Phi}_{n_\rho,n_z,\Lambda,\Sigma}\left(\overrightarrow{R},\sigma\right)=\frac{1}{2\pi^{3/2}}\int d\overrightarrow{R}e^{-i\,\overrightarrow{K}\cdot\overrightarrow{R}}\Phi_{n_\rho,n_z,\Lambda,\Sigma}\left(\overrightarrow{R},\sigma\right) \tag{24}$$

normalized to one.

We define densities $n_i\left(\overrightarrow{K}\right)$ in momentum space in an analogous way of that in the configuration space:

$$\rho_i\left(\overrightarrow{R}\right)=\rho_i\left(r,z\right)=\left|\Phi_i^+\left(r,z\right)\right|^2+\left|\Phi_i^-\left(r,z\right)\right|^2, \tag{25}$$

with

$$\Phi_i^\pm\left(r,z\right)=\frac{1}{\sqrt{2\pi}}\sum_{n_\rho,n_z,\Lambda,\Sigma}\delta_{\Sigma,\pm\frac{1}{2}}\delta_{\Lambda,\pm\Lambda}C^i_{n_\rho,n_z,\Lambda,\Sigma}\Phi_{n_\rho,n_z,\Lambda,\Sigma}\left(\overrightarrow{R},\sigma\right), \tag{26}$$

and

$$n_i\left(\overrightarrow{K}\right)=n_i\left(k,k_z\right)=\left|\widetilde{\Phi}_i^+\left(k,k_z\right)\right|^2+\left|\widetilde{\Phi}_i^-\left(k,k_z\right)\right|^2, \tag{27}$$

with

$$\widetilde{\Phi}_i^\pm\left(k,k_z\right)=\frac{1}{\sqrt{2\pi}}\sum_{n_\rho,n_z,\Lambda,\Sigma}\delta_{\Sigma,\pm\frac{1}{2}}\delta_{\Lambda,\pm\Lambda}C^i_{n_\rho,n_z,\Lambda,\Sigma}\widetilde{\Phi}_{n_\rho,n_z,\Lambda,\Sigma}\left(\overrightarrow{K},\sigma\right). \tag{28}$$

These single particle momentum distributions $n_i\left(\overrightarrow{K}\right)$ were averaged over nuclear symmetry axis directions.

Similarly to the total density

$$\rho\left(\overrightarrow{R}\right)=\sum_i 2\upsilon_i^2\rho_i\left(\overrightarrow{R}\right), \tag{29}$$

the total momentum distribution is given by

$$n\left(\overrightarrow{K}\right)=\sum_i 2\upsilon_i^2 n_i\left(\overrightarrow{K}\right), \tag{30}$$

where υ_i^2 is the occupation probability resulting from the BCS model. [11], [10]

The results for the occupation number calculations are shown in Fig. 2.

The energies of the ^{238}U proton bound states are shown in table 1.

IV. FISSILITY

The quasifree knockout of nucleons leads to the excitation of the residual nucleus. This excitation energy (E^*, nucleus A-1) has two origins: holes in the shells of the nucleus A, which appear as a result of the knockout of nucleons, and final state interaction (FSI) of the outgoing nucleon, which we assume as negligeable due to the high energy of the proton.

The fast, quasi free reaction stage occurs at zero thermal excitation (ground state) of the initial nucleus ^{238}U, and results in a single hole in one of the shells. This single hole configuration forms a doorway for a thermalization process which leads to the thermal excitation $E^*$of the residual nucleus ^{237}Pa.

The thermalization is a complicate process which involves creation of new many particle-hole configurations in competition with particles emission and fission, and for some doorway configurations it might has non statistical character, but, as a first guide-line for order of magnitude estimates we calculate the total fission probability (nucleus with energy E^* deexcites in several steps) on the statistical theory grounds, both with and without taking into account the preequilibrium decay.

A. Compound nucleus model

Firstly, we considered a extreme situation, by assuming that the residual interaction leads to thermalization and formation of compound nucleus just after the fast reaction stage, without any preequilibrium particle emission In this case, the compound nucleus excitation energy is assumed to be :

$$E^* = -E_\alpha \tag{31}$$

where E_α is the energy of the bound state (hole).

For calculations of compound nucleus fissility we used the Bohr Wheeler [12] and Weisskopf [13] models for the description of the evaporation/fission competition. It was developed a Monte Carlo algorithm for the evaporation/fission processes which includes not only the neutron evaporation vs. fission competition, but also takes into account the proton and alpha-particle contributions.

The probability for the emission of a particle j with kinetic energy between E_k and $E_k + dE_k$ is calculated within the Weisskopf statistical model [13] as:

$$P_f(E_k)dE_k = \gamma_j \sigma_j E_k \left(\frac{\rho_f}{\rho_i}\right) dE_k, \tag{32}$$

where σ_j is the nuclear capture cross section for the particle j, $\gamma_j = \frac{gm}{\pi^2\hbar^3}$, where g denotes the number of spin states, and m is the particle mass. The level densities for the initial and final nucleus, ρ_i and ρ_f, respectively, are calculated from the Fermi gas expression

$$\rho(E_j^*) = \exp\left[2(\, aE_j^*)^{1/2}\right],$$

where a is the level density parameter (see below),

$$E_j^* = E^* - (B_j + V_j), \tag{33}$$

E^* is the nuclear excitation energy in the initial state, B_j is the particle separation energy, and V_j is the Coulomb barrier corrected for the nuclear temperature, τ, defined by $E^* = a\tau^2$.

The particle emission width is calculated as

$$\Gamma_j = \int_0^{E_j^*} P_j(E_k)dE_k. \tag{34}$$

From this general equation, the k-particle emission probability relative to the j-particle emission is:

$$\frac{\Gamma_k}{\Gamma_j} = \left(\frac{\gamma_k}{\gamma_j}\frac{E_k^*}{E_j^*}\frac{a_j}{a_k}\right) \exp\left[2\left((a_k\, E_k^*)^{1/2} - \left(a_j E_j^*\right)^{1/2}\right)\right]. \tag{35}$$

The level density parameter for neutron emission is [14]:

$$a_n = (0.134\ A - 1.21\ \cdot 10^{-4}\ A^2)\ \mathrm{MeV}^{-1}, \tag{36}$$

and for all other particle emission this quantity is related to a_n by,

$$a_j = r_j a_n, \tag{37}$$

where r_j is an adimensional constant.

Shell model corrections [15] are not taken into account. For high excitation energies their effects are likely to cancel each other upon averaging over all possible nuclei created during the reaction.

Using the fission width from the liquid drop model [12], and the neutron emission width from Weisskopt [13], we get

$$\frac{\Gamma_f}{\Gamma_n} = K_f\ \exp\left[2\left(\left(a_f\ E_f^*\right)^{1/2} - \left(a_n\ E_n^*\right)^{1/2}\right)\right], \tag{38}$$

where

$$K_f = K_0\ a_n \frac{2((a_f\ E_f^*)^{1/2} - 1}{4A^{2/3} a_f E_n^*}, \tag{39}$$

with $K_0 = 14.39$ MeV and $E_j^* = E^* - B_f$. Here B_f is the fission barrier height discussed below.

For proton emission we get

$$\frac{\Gamma_p}{\Gamma_n} = \left(\frac{E_p^*}{E_n^*}\right) \exp\left[2\,(a_n)^{1/2}\left(\left(r_p E_p^*\right)^{1/2} - (E_n^*)^{1/2}\right)\right], \tag{40}$$

and for alpha-particle emission [16] [14],

$$\frac{\Gamma_a}{\Gamma_n} = \left(\frac{2\ E_a^*}{E_n^*}\right) \exp\left[2(a_n\ )^{1/2}((r_a E_a^*)^{1/2} - (E_n^*)^{1/2})\right]. \tag{41}$$

In the above equations, the Coulomb potential for protons is [17]

$$V_p = \ C\frac{k_p(Z-1)e^2}{r_0(A-4)^{1/3} + R_p}, \tag{42}$$

and for alphas,

$$V_a = C\frac{2K_a(Z-2)e^2}{r_0(A-4)^{1/3}+R_a}, \tag{43}$$

where $K_p = 0.70$ and $K_a = 0.83$ are the Coulomb barrier penetrability for protons and alpha particles, respectively, $R_p = 1.14$ fm is the proton radius ,$R_a = 2.16$ fm is the alpha particle radius, and $r_0 = 1.2\ fm$. The factor C introduces in a semi-empirical way the dynamical effects in particle separation energy and fission barrier due to the nuclear temperature [17], namely

$$C = 1 - \frac{E^*}{B}\ , \tag{44}$$

where B is the total nuclear binding energy (B=1794 MeV for ^{237}Pa [17]).

The fission barrier is calculated by [17],

$$B_f = C(0.22(A-Z) - 1.40Z + 101.5)\ \text{MeV}. \tag{45}$$

The neutron separation energy was taken as 5.78 MeV for the first step (^{237}Pa) , and for the other steps as [15]:

$$B_n = \ (-0.16(A-Z) + 0.25Z + 5.6)\ \text{MeV}, \tag{46}$$

while the proton and alpha-particle separation energies are calculated through the nuclear mass formula [18]:

$$B_p = m_p + M(A-1, Z-1) - M(A,Z), \tag{47}$$

where m_p is the proton mass, and $M(A,Z)$ is the nuclear mass calculated with the parameters from reference [18]. For the alpha particles we get

$$B_a = m_a + M(A-4, Z-2) - M(A,Z), \tag{48}$$

where m_a is the alpha particle mass.

These values reproduce the experimental data for P_f (see discussion below)

The present Monte Carlo code for evaporation-fission calculates, at each step i of the evaporation chain, the fission probability, F_i, defined as

$$F_i = \frac{(\frac{\Gamma_f}{\Gamma_n})_i}{1 + (\frac{\Gamma_f}{\Gamma_n})_i + (\frac{\Gamma_p}{\Gamma_n})_i + (\frac{\Gamma_\alpha}{\Gamma_n})_i},$$

An evaporating particle j is randomly chosen (neutron, proton or alpha particle), according to its relative branching ratios. Once one of these particles is chosen , the mass and atomic numbers are recalculated through

$$A_{i+1} = A_i - \Delta A_i,$$

and

$$Z_{i+1} = Z_i - \Delta Z_i,$$

where ΔA_i, and ΔZ_i, are, respectively, the mass and atomic numbers of the ejected particle at the *ith* step in the evaporation process. The nuclear excitation energy is modified according to the expression

$$E^*_{i+1} = E^*_i - B_i - T_i,$$

where B_i and T_i are the separation and the asymptotic kinetic energies of the particle being ejected, respectively. For neutrons $T = 2$ MeV, and for protons and alpha particles $T = 0$ MeV. The expressions described above ensure that the nuclear excitation energy will be, at each step in the evaporation chain, smaller than in the previous step. This process continues until the excitation energy available in the nucleus is not enough to emit any one of the possible evaporating particles. At this point the evaporation process stops, and we can calculate the nuclear fissility by the expression

$$W = \sum_i \left[\prod_{j=0}^{i-1} (1 - F_j) \right] F_i. \tag{49}$$

Using the model described above, we calculated the fissility for ^{237}Pa (figure 3, solid curve). Peaks observed for the fissility reflect the opening of the fission channel in the

daughter nuclei. Figure 3 also shows (rectangle) the data for the fissility of ^{237}Pa obtained by extrapolation of the neutron to fission widths ratios for $Z = 91$, and $A = 230, 231, 232, 233$ to $A = 237$ [19], by using the empirical trend presented in Vandenbosch and Huizenga [16]

It should be pointed out that in our calculations of the fissility we assumed that the hole excitation energies for an A-1 nucleus correspond to the compound nucleus excitation energies , that is to say, the complete thermalization is reached without any preequilibrium decay. Such calculations could be considered as an upper limit estimate for the fissility.

B. Exciton model

During the thermalization of the hole excitation energy, the nucleus $A-1$ could undergo particle evaporation (preequilibrium decay [20], [21]).

In this case, the energy of the hole is not attributed to the nuclear temperature but, instead, assumed as a characteristic of the doorway state in the thermalization process followed by the emission of particles or fission.

The calculation involving the preequilibrium decay was performed within the framework of the exciton model [22], using the code STAPRE. In this model, the states of the system are classified according to the number of excitons n, which corresponds to the total number of excited particle p and hole h degrees of freedom, $n = p + h$. The exciton model included in STAPRE does not distinguish between protons and neutrons. Starting from a simple configuration of low exciton number, the system is assumed to equilibrate through a series of two-body collisions and to emit particles from all intermediate states. The application of a two-body interaction to the states of a (p, h) configuration results in states with $(p+1, h+1)$, (p, h), and $(p-1, h-1)$ excited particles and holes. The difference between the number of excited particles and holes remains fixed, justifying the use of the exciton number to label the states. However, the transition rates, which are an averaging over all states of a configuration, do depend on the number of excited particles and holes. The equation

governing the time development of the occupation $P(n)$ of the $n-th$ exciton configuration can thus be written as

$$\frac{dP(n)}{dt} = \lambda_{-}(n+2)\,P(n+2) + \lambda_0(n)\,P(n) + \lambda_{+}(n-2)\,P(n-2) - \lambda(n)\,P(n) \qquad (50)$$

where $\lambda(n)$ is the total transition rate,

$$\lambda(n) = \lambda_{-}(n) + \lambda_0(n) + \lambda_{+}(n) + \lambda_e(n), \qquad (51)$$

with $\lambda_e(n)$ being the total rate of particle emission from the $n-th$ exciton configuration. The quantities $\lambda_{-}(n)$, $\lambda_0(n)$, and $\lambda_{+}(n)$ are the average rates for internal transitions from the $n-th$ exciton configuration with a change of exciton numbers by -2, 0, or +2.

The internal transition rates can be written as the product of the average squared matrix element of the residual interaction $|M|^2$with the relative density of available states. For the latter, STAPRE uses the expressions of Williams [23] as corrected for the Pauli principle by Cline [24]. These yield

$$\begin{aligned}
\lambda_{-}(n) \equiv \lambda_{-}(p,h,E) &= \frac{2\pi}{\hbar}|M|^2\frac{g\left(gE - C_{p+1,h+1}\right)^2}{p+h+1}, \qquad (52)\\
\lambda_0(n) \equiv \lambda_0(p,h,E) &= \frac{2\pi}{\hbar}|M|^2 g(p+h-1)\left(gE - C_{p,h}\right),\\
\lambda_{+}(n) \equiv \lambda_{+}(p,h,E) &= \frac{2\pi}{\hbar}|M|^2 gph(p+h-2),
\end{aligned}$$

where

$$C_{p,h} = \frac{1}{2}\left(p^2 + h^2\right),$$

with E the excitation energy of the system. The parameter g is the single-particle state density, which is taken to be $g = \frac{6}{\pi^2}a$, with a as the level density parameter. Following Kalbach-Cline [25], the average matrix element is approximated as

$$|M|^2 = \frac{f_M}{A^3 E},$$

where A is the mass number of the system and f_M is a parameter, which we assumed to be $f_M = 230$ MeV^3 in our calculations.

The particle emission rate $\lambda_e(n)$ is the sum of the integrated proton and neutron differential emission rates, $\lambda_{e\nu}(n,\varepsilon)\,d\varepsilon_\nu$, which are determined through considerations of detailed balance [26],

$$\begin{aligned}\lambda_{e\nu}(n,\varepsilon)\,d\varepsilon_\nu &\equiv \lambda_{e\nu}(p,h,E,\varepsilon_\nu)\,d\varepsilon_\nu \\ &= \frac{1}{\pi^2\hbar^3}\mu_\nu\,\varepsilon_\nu\,\sigma_\nu(\varepsilon_\nu)\,R_\nu\frac{\omega(p-1,h,E-B_\nu-\varepsilon_\nu)}{\omega(p,h,E)}\,d\varepsilon_\nu,\end{aligned} \tag{53}$$

where μ_ν is the reduced mass of the emitted neutron/proton, ε_ν its outgoing kinetic energy, B_ν its separation energy, and $\sigma_\nu(\varepsilon_\nu)$ is the cross section for the inverse absorption process. The factor R_ν is a simple correction standing for the fact that neutrons and protons have not been distinguished in the process; thus,

$$R_\nu = \begin{cases} N/A & \text{for neutron emission} \\ Z/A & \text{for proton emission} \end{cases}.$$

The densities of states are taken to be the Williams densities,

$$\omega(p,h,E) = \frac{g\ (gE - A_{p,h})^{p+h-1}}{p!\,h!\,(p+h-1)!}, \tag{54}$$

where the Pauli blocking correction is

$$A_{p,h} = \frac{1}{4}\left(p^2+h^2+p-3h\right).$$

The differential emission rates differ from those of usual Weisskopf compound nucleus emission by the factor R_ν and by the use of exciton state densities rather than compound nucleus ones.

The time evolution equation, Eq. (50), form a set of coupled linear differential equations whose solution could be written in the form of a vector as,

$$\vec{P}(t) = \exp\left[-\Lambda\,t\right]\,\vec{P}_0,$$

where the matrix Λ is given by

$$\Lambda_{nn'} = \lambda(n)\,\delta_{n',n} - \lambda_-(n+2)\,\delta_{n',n+2} - \lambda_0(n)\,\delta_{n',n} - \lambda_+(n-2)\,\delta_{n',n-2},$$

and the vector $\vec{P}_0$ describes the initial exciton configuration of the system,

$$P_0(n) \equiv P_0(p,h) = \delta_{p,p_0}\delta_{h,h_0}.$$

The decay of the system into all possible final configurations can be obtained by integrating the total emission rate over all time,

$$\sum_n \int_0^\infty \lambda_e(n)\, P(n,t)\, dt = \sum_{n,n'} \lambda_e(n)\, \left(\Lambda^{-1}\right)_{n,n'} P_0(n'). \tag{55}$$

The decay of the fraction of the initial probability, which survives preequilibrium emission, is described using the Hauser-Feshbach formalism. We have considered fission in competition with neutron and gamma emission.

The initial configuration in ^{237}Pa consists of one-particle at the Fermi level and one-hole in a bound state. This configuration is consistent with the proton knockout reaction for ^{238}U initiating the statistical cascade. Our calculations were performed assuming an one -hole initial configuration of the l=0 partial wave alone. The particle at the Fermi level contributes negligibly to the equilibration process. The fission barriers, neutron separation energies and level density parameters were taken the same as those of the compound nucleus calculations in the previous section.

The exciton model fissility results for single hole states of ^{237}Pa are shown in fig 3 by the dotted curve. We note that these calculations for fissility show a smoother behavior than that for compound model. The preequilibrium particle emission removes some excitation energy before a equilibrium is reached reducing, therefore, the probability of opening new chances for fission.

V. FINAL RESULTS

The differential cross section for the $(e,e'pf)$-reaction was obtained by assuming an isotropic angular distribution for the fission fragments, and the fissility as a factor :

$$\frac{d^7\sigma}{d\Omega_e\ d\Omega_p\ dE_p\ d\Omega_f} = \frac{1}{4\pi}\frac{d^5\sigma}{d\Omega_e\ d\Omega_p\ dE_p} P_f \tag{56}$$

Fig. 4 shows the seven folded differential cross sections $\frac{d^7\sigma}{d\Omega_e\ d\Omega_p\ dE_p\ d\Omega_f}$ for some bound proton states (table 1) and the compound nucleus model fissility (solid curve in fig.3) calculated for ε_1=2000 MeV , $\theta e = 23^0$ and the parallel kinematics [27]. In this kinematics ε_1 and θe are fixed, and for each value of ε_2 the proton spectrum is measured in the direction of $\vec{q}$, varying each time the angle $\theta_{P_p k_1}$.(see fig.1). For such scheme of measurements the initial (missing) momentum of the proton $\vec{p_m}$ is always parallel (or antiparallel) to $\vec{q}$. The parallel kinematics simplify the accounting of FSI, since there are no contribution of interference terms in the cross sections (see Eqs. (9)). Figs 5 and 6 show the momentum distributions for states used in the calculation of the cross sections presented in fig. 4, and fig. 7 shows the outgoing proton kinetic energy and angle θ_{Ppk_1} versus ε_2 for the parallel kinematics we use.

Figs. 8 and 9 show the differential $(e,e'pf)-$cross sections calculated for the same ε_1 and θe but for two fixed proton angles: $\theta_{P_p k_1} = 0.98$ rad for the group of proton states of ^{238}U which have a maximum in the low missing momentum region (fig.5), and $\theta_{P_p k_1} = 0.82$ rad for the group having a maximum in the high missing momentum region (fig.6) . These angles $\theta_{P_p k_1}$were chosen in order to achieve parallel kinematics, that is $\theta_{P_p q} \approx 0$, and maximum for cross sections at both the low ($\theta_P = 0.98$ rad) and high ($\theta_P = 0.82$ rad) missing momentum regions. Fig.10 shows the missing momentum P_m and the angle $\theta_{P_p q}$ as functions of the outgoing proton kinetic energy for $\theta_p = 0.98$ rad (solid curve) and 0.83 rad (dashed curve).

It is seen from the figures 8,9 and 10 that for such a choice the cross sections have maxima at E_p around 300 and 400 MeV and, for these energies, the proton angles $\theta_{P_p q}$ are small (parallel kinematics).

The differential cross-sections presented in figures 4, 8 and 9 correspond to the situation when the hole excitation energies for an A-1 nucleus is the compound nucleus excitation energies , that is to say, the complete thermalization is reached without any preequilibrium

decay. Such calculations could be considered as an upper limit estimate for the cross section

VI. CONCLUSIONS

We presented a theoretical study for the quasifree electrofission of ^{238}U.

The proton bound states were calculated in the framework of the Macroscopic-Microscopic approach, using the axially deformed Woods-Saxon single particle potential. The occupation numbers were calculated in the BCS approach.

The exclusive differential cross sections for the quasi free scattering reaction stage were calculated in PWIA using off-shell electron-nucleon cross sections.

The fissility for the single hole states of the residual nucleus ^{237}Pa was calculated in the framework of two approaches: compound nucleus model without taking into account the preequilibrium emission of the particles, and the exciton model accounting for preequilibrium emission. Both models exhibit the same general trend, but the fissility as given by the preequilibrium model is smoother.

The obtained results could serve as a first guide-line on order of magnitude estimates of the expected cross sections for quasi free electrofission of ^{238}U.

VII. ACKNOWLEDGMENTS

The authors thank the Brazilian agencies CNPq and FAPESP for the partial support to this work and the graduate students W.R. Carvalho, M.S. Vaudeluci and L.F.R. Macedo for their help.

REFERENCES

[1] L.S.Cardman, Nucl.Phys.**A654**(1999)73

[2] V.P. Likhachev et al, Contribution of quasielastic scattering to the inclusive electrofission cross section of uranium at E_0 =90-250 MeV, Phys. Rev.C, to be submitted

[3] K.Hansen et al, Phys.Rev. **C41**(1990)1619

[4] T. de Forest, Nucl. Phys. **A392** (1983) 232

[5] F. Garcia, O. Rodriguez, J. Mesa, J.D.T. Arruda-Neto, V.P.Likhachev, E. Garrote, R. Capote and F. Guzmán.Comp. Phys. Commun., **120** (1999) 57

[6] V.V. Pashkevich, Nucl. Phys. **A169** (1971) 275

[7] F.A. Ivanyuk, H. Hofmann, V.V. Pashkevich, S. Yamaji, Phys. Rev. **C55** (1997)1730

[8] F. Garcia, E. Garrote, M.-L. Yoneama, J.D.T. Arruda-Neto, J. Mesa, F. Bringas, J.F. Dias, V.P. Likhachev, O. Rodriguez and F. Guzmán, Eur. Phys. J. A **6**, 49 (1999)

[9] V.A. Chepurnov, Sov. J. Nucl. Phys. **6**, 696 (1968)

[10] F. Garcia, O. Rodriguez, V.A. Rubchenya, E. Garrote, Comp. Phys. Commun. **86** (1995) 129

[11] F. Garcia, O. Rodriguez, E. Garrote and E. Lopez, J. Phys. G: Nucl. Part. Phys., **19** (1993) 2157

[12] N. Bohr and J. A. Wheeler, Phys. Rev. 56 (1939) 426

[13] V. Weisskopf, Phys. Ver. 72 (1947) 1114

[14] A. S.Iljinov et al, Nucl. Phys. 32 (1980) 166

[15] C. Guaraldo et al., Il Nuovo Cim. 103 (1990) 607

[16] R. Vandenbosch and J. R. Huizenga in Nuclear Fission, pp 227, 1^{a}Ed., New York Aca-

demic Press, 1973

[17] O. A. P. Tavares and M. L. Terranova, Z. Phys.: Hadr. And Nucl. 343 (1992) 407

[18] E. Segrè in "Nuclei and Particles: An Introduction to Nuclei anda Subnuclei Physics", pp 215, 3ªEd., W. A. Benjamin, INC, 1965

[19] A Gavron et al, Phys.Rev. **C13,** 2374 (1976)

[20] R.Bonetti, M.B. Chadwick, P. E. Hodgson, B.V. Carlson and M.S. Hussein, Phys. Rep. 202 (1991) 171

[21] E.Gadioli and P.E. Hodgson, "Pre-equilibrium Nuclear Reactions " Oxford Univ. Press, 1992

[22] C. Kalbach, Acta phys. slov. 25 (1975) 100

[23] F.C. Williams Jr., Phys. Lett. 31B (1970) 184

[24] C.K. Cline, Nucl. Phys. A186 (1972) 273

[25] C. Kalbach-Cline, Nucl. Phys. 210 (1973) 590

[26] C.K. Cline, Nucl. Phys. **A186** (1972) 273

[27] J.Potter, Nucl. Phys. **45,** 33 (1963)

VIII. TABLE 1

	[MeV]	πJ	[N n_z Λ]		[MeV]	πJ	[N n_z Λ]		[MeV]	πJ	[N n_z Λ]
1	-33.685	1/2	1/2 [0 0 0]	23	-16.192	-3/2	3/2 [3 0 1]	45	-7.491	3/2	3/2 [4 0 2]
2	-31.397	-1/2	1/2 [1 1 0]	24	-15.490	-1/2	1/2 [3 0 1]	46	-7.195	1/2	1/2 [4 0 0]
3	-30.043	-3/2	3/2 [1 0 1]	25	-15.415	7/2	7/2 [4 1 3]	47	-6.277	5/2	5/2 [6 4 2]
4	-29.670	-1/2	1/2 [1 0 1]	26	-14.529	9/2	9/2 [4 0 4]	48	-6.189	-5/2	5/2 [5 2 3]
5	-28.141	1/2	1/2 [2 2 0]	27	-14.302	3/2	3/2 [4 2 2]	49	-5.348	-3/2	3/2 [5 2 1]
6	-26.630	3/2	3/2 [2 1 1]	28	-13.984	-1/2	1/2 [5 3 0]	50	-4.827	7/2	7/2 [6 3 3]
7	-25.963	1/2	1/2 [2 1 1]	29	-13.111	1/2	1/2 [4 2 0]	51	-4.340	-7/2	7/2 [5 1 4]
8	-25.542	5/2	5/2 [2 0 2]	30	-13.091	-3/2	3/2 [5 4 1]	52	-3.949	-1/2	1/2 [5 2 1]
9	-24.473	3/2	3/2 [2 0 2]	31	-12.383	5/2	5/2 [4 1 3]	53	-3.667	1/2	1/2 [6 5 1]
10	-24.025	-1/2	1/2 [3 3 0]	32	-11.735	-5/2	5/2 [5 3 2]	54	-3.465	-5/2	5/2 [5 1 2]
11	-22.836	1/2	1/2 [2 0 0]	33	-11.053	7/2	7/2 [4 0 4]	55	-3.417	9/2	9/2 [6 2 4]
12	-22.716	-3/2	3/2 [3 2 1]	34	-10.831	3/2	3/2 [4 1 1]	56	-3.051	-9/2	9/2 [5 0 5]
13	-21.614	-1/2	1/2 [3 2 1]	35	-10.388	-1/2	1/2 [5 4 1]	57	-2.261	11/2	11/2 [6 1 5]
14	-21.292	-5/2	5/2 [3 1 2]	36	-10.280	-7/2	7/2 [5 2 3]	58	-2.207	-1/2	1/2 [7 5 0]
15	-20.333	-7/2	7/2 [3 0 3]	37	-9.794	1/2	1/2 [4 1 1]	59	-2.182	7/2	7/2 [5 0 3]
16	-19.621	-3/2	3/2 [3 1 2]	38	-9.301	5/2	5/2 [4 0 2]	60	-1.773	3/2	3/2 [6 4 2]
17	-19.254	1/2	1/2 [4 2 0]	39	-9.054	-9/2	9/2 [5 1 4]	61	-1.669	1/2	1/2 [6 4 0]
18	-18.229	-5/2	5/2 [3 0 3]	40	-8.356	-3/2	3/2 [5 3 2]	62	-1.553	-3/2	3/2 [7 4 1]
19	-18.189	3/2	3/2 [4 3 1]	41	-8.276	1/2	1/2 [6 4 0]	63	-1.459	13/2	13/2 [6 0 6]
20	-18.130	-1/2	1/2 [3 1 0]	42	-8.217	-11/2	11/2 [5 0 5]	64	-1.118	-3/2	3/2 [5 1 2]
21	-16.730	5/2	5/2 [4 2 2]	43	-7.624	-1/2	1/2 [5 3 0]	65	-1.065	-1/2	1/2 [5 1 0]
22	-16.416	1/2	1/2 [4 3 1]	44	-7.597	3/2	3/2 [6 5 1]	66	-0.393	-5/2	5/2 [7 5 2]

IX. FIGURE CAPTIONS

Fig.1. Momentum diagram of the $A(e,e'p)A-1$ reaction in the impulse approximation: $\overrightarrow{k}_1$, and $\overrightarrow{k}_2$ are the initial and final electron momenta, respectively; $\overrightarrow{p}_m$ is the momentum of proton before interaction; $\overrightarrow{p_p}$ is the momentum of

knocked-out proton.

Fig.2. Occupation probabilities for the single particle bound states of ^{238}U.

Fig.3. Fissility of ^{237}Pa vs the hole excitation energy.

The solid curve shows the compound nucleus model calculation, assuming that the hole excitation energies correspond to the compound nucleus

excitation energies: the complete thermalization is reached without any preequilibrium decay. The dotted curve corresponds to the exciton model

calculations, which take into account the preequilibrium decay. The rectangle shows the extrapolated experimental data (se text for details).

Fig. 4. Seven folded differential cross sections for the parallel kinematics. The calculations of the cross sections were accomplished for $\varepsilon_1 = 2000$

MeV, $\theta e = 23^0, \phi = 0^0$. The cross section for E=-10.388 MeV state (subbarier) is multiplied by 100.

Fig.5. Momentum distributions for some proton bound states having maxima at the low missing momentum region.

Fig.6. Momentum distributions for some proton bound states having maxima at the high missing momentum region.

Fig. 7. Variation of the angle $\theta_{p_p k_1}$ (see fig.1) and the outgoing proton kinetic energy E_p vs ε_2 for the parallel kinematics and $\varepsilon_1 = 2000$ MeV, $\theta e = 23^0$.

Fig.8. Differential cross sections for some bound states of ^{238}U, having maxima of the momentum distributions at the low missing momentum region. The calculations of the cross sections were accomplished for $\varepsilon_1 = 2000$ MeV, $\theta e = 23^0, \phi = 0^0$ and $\theta_{p_p k_1} = 0.98$ rad.

Fig.9. The same as in figure.5, but for some bound states of ^{238}U, having maxima of the

momentum distributions at the high missing momentum region and for $\theta_{p_p k_1} = 0.82$ rad .

Fig.10. Missing momentum p_m and angle $\theta_{P_p q}$ as functions of the outgoing proton kinetic energy for $\theta_{p_p k_1} = 0.98$ rad (solid curve) and 0.83 rad (dashed curve).

X. TABLE CAPTION

Table 1: Proton single-particle levels of ^{238}U. The Fermi level is the level 46.

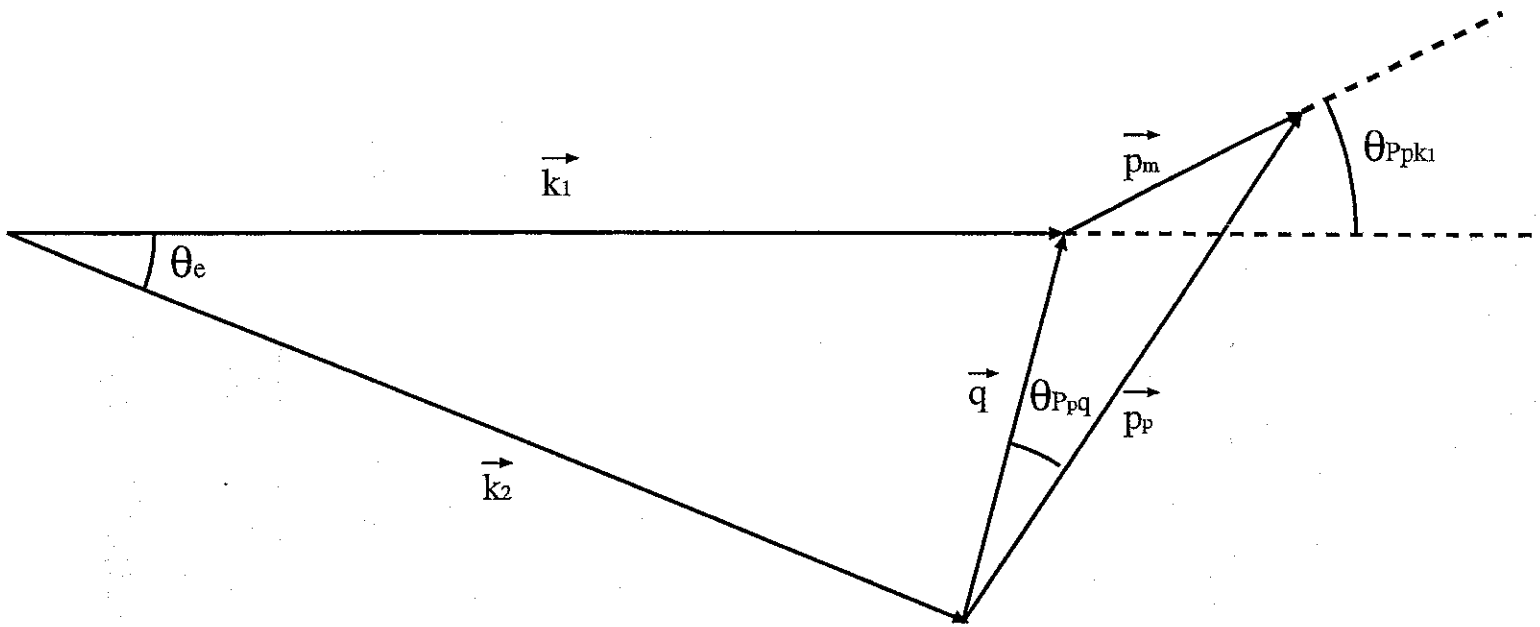

Fig 1

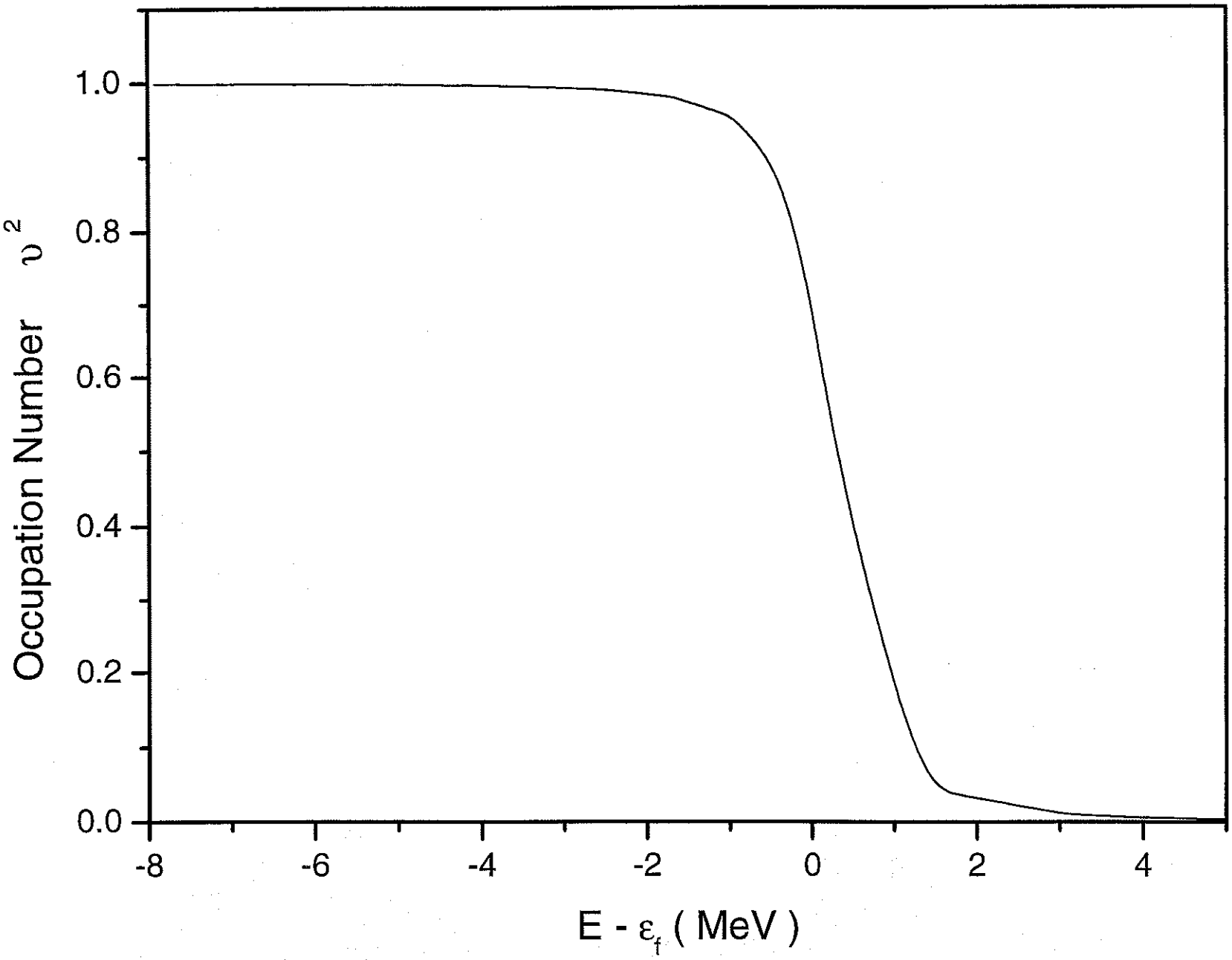
Occupation Number v^2
1.0
0.8
0.6
0.4
0.2
0.0
-8
-6
-4
-2
0
2
4
E - ε_f (MeV)

Fig 2

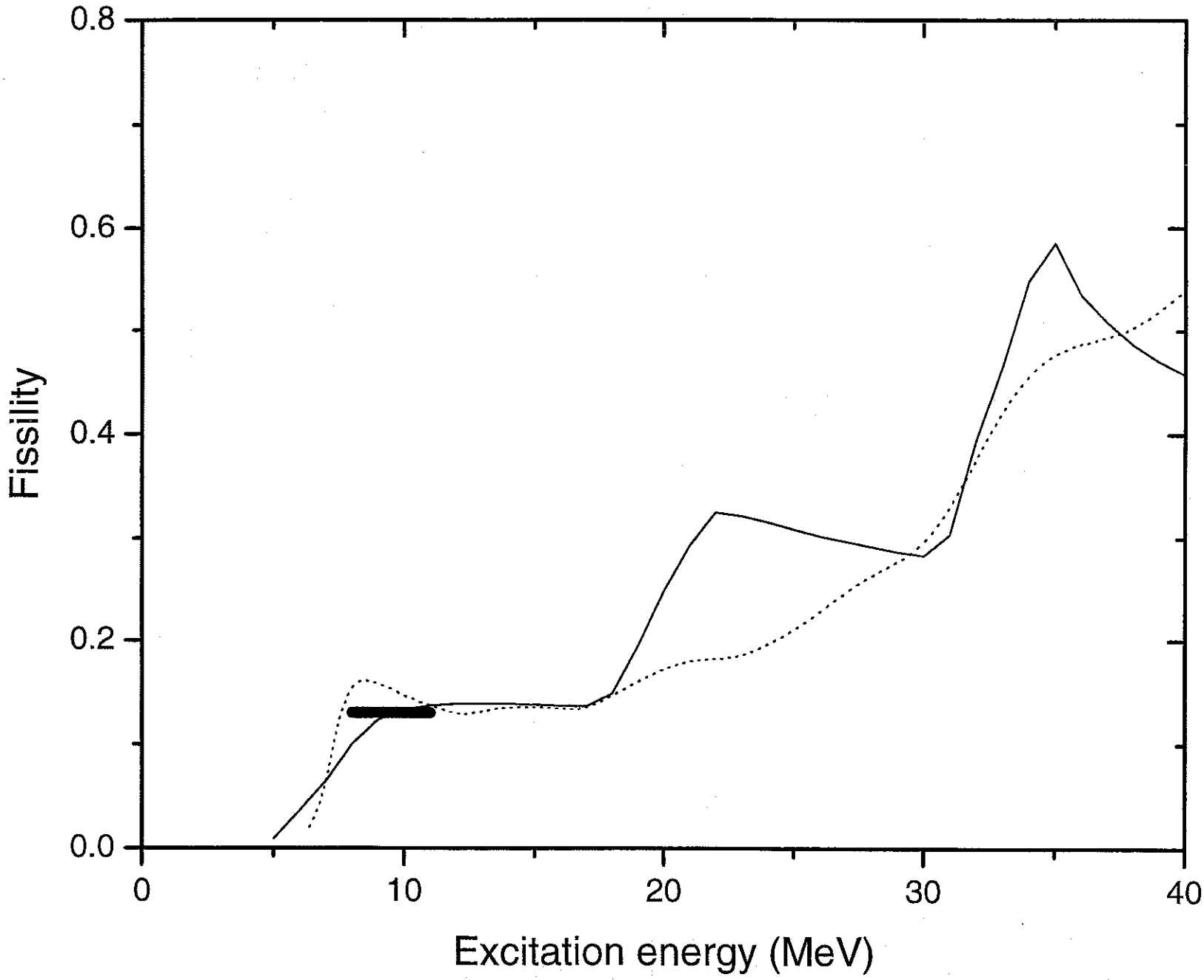

Fig 3

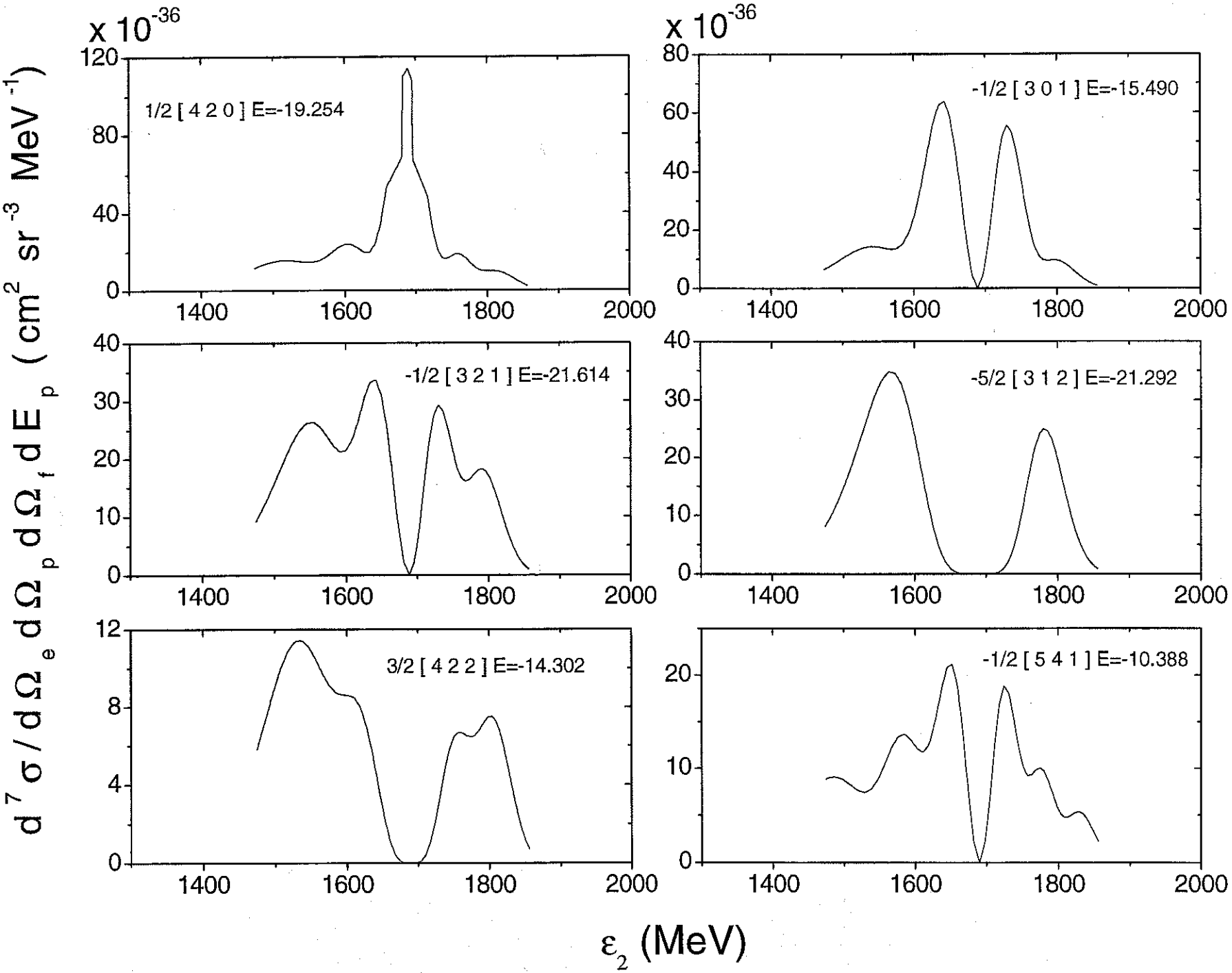
x 10^-36
1/2 [4 2 0] E=-19.254
x 10^-36
-1/2 [3 0 1] E=-15.490
-1/2 [3 2 1] E=-21.614
-5/2 [3 1 2] E=-21.292
3/2 [4 2 2] E=-14.302
-1/2 [5 4 1] E=-10.388
d^7σ / dΩ_e dΩ_p dΩ_f dE_p (cm^2 sr^-3 MeV^-1)
ε_2 (MeV)

Fig 4

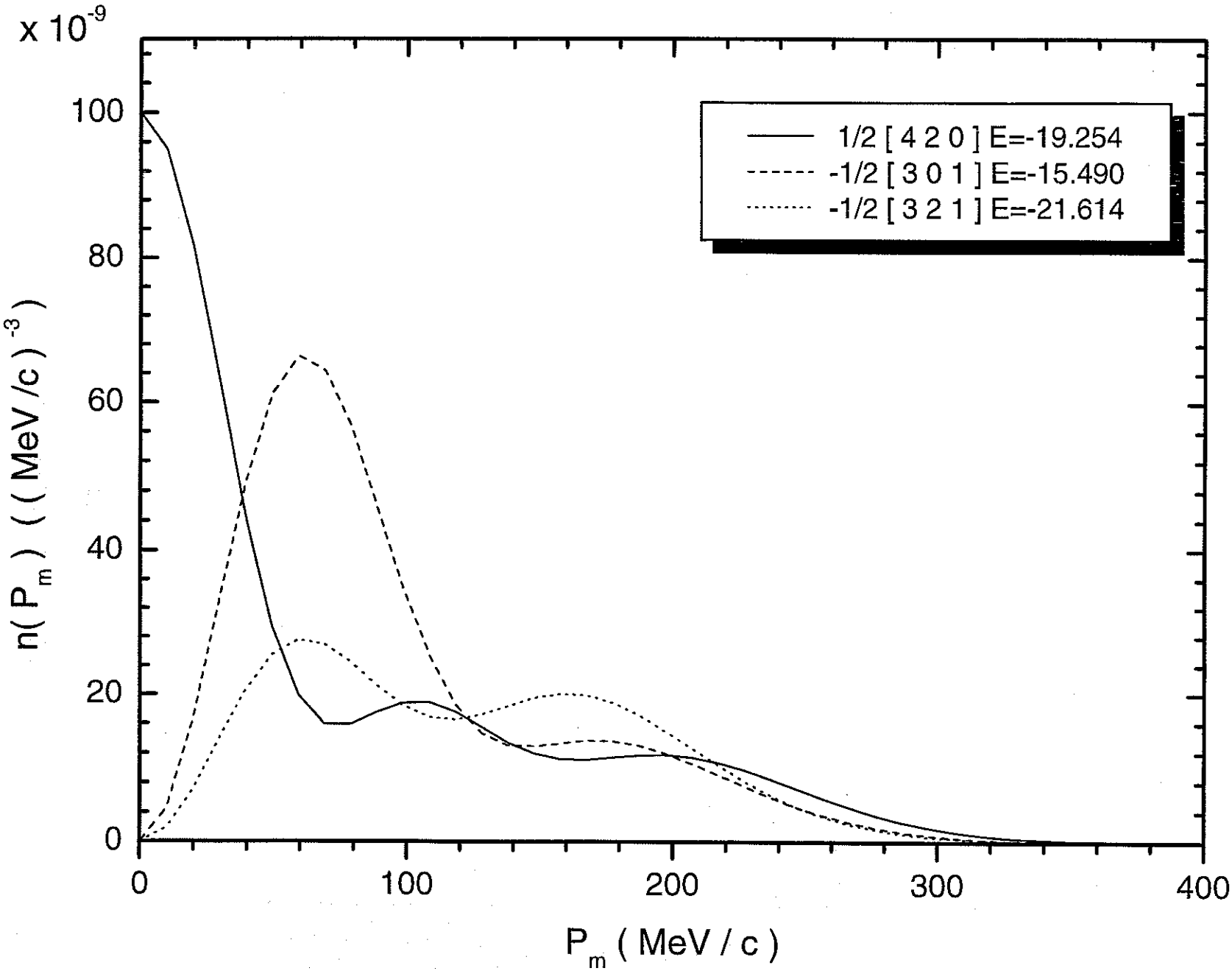
x 10^-9
100
80
60
40
20
0
n(P_m) ((MeV /c) ^-3)
0
100
200
300
400
P_m (MeV / c)
1/2 [4 2 0] E=-19.254
-1/2 [3 0 1] E=-15.490
-1/2 [3 2 1] E=-21.614

Fig 5

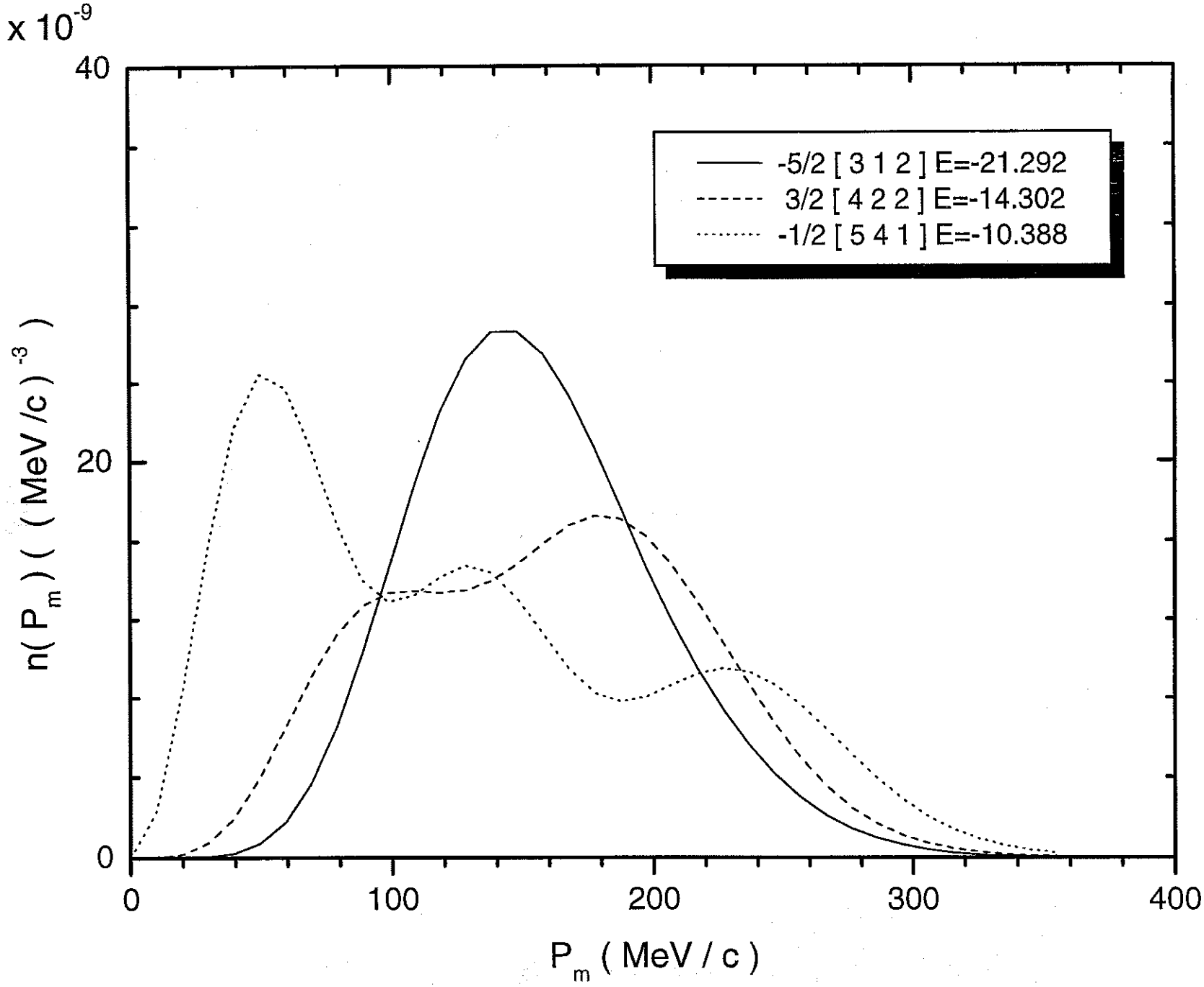
x 10^-9
40
20
0
0
100
200
300
400
n(P_m) ((MeV /c) ^-3)
P_m (MeV / c)
-5/2 [3 1 2] E=-21.292
3/2 [4 2 2] E=-14.302
-1/2 [5 4 1] E=-10.388

Fig 6

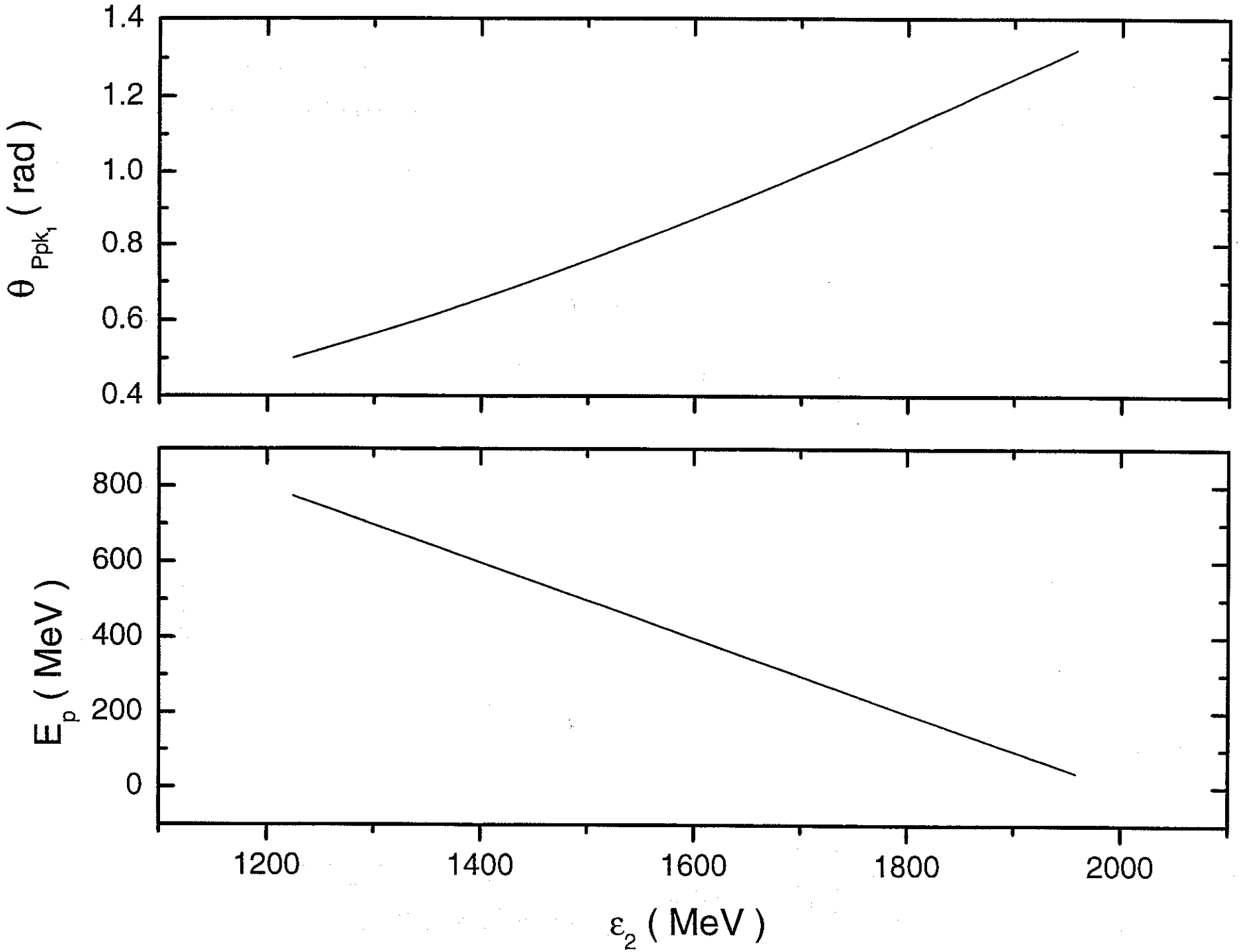
1.4
1.2
1.0
0.8
0.6
0.4
θ Ppk1 (rad)
800
600
400
200
0
Ep (MeV)
1200
1400
1600
1800
2000
ε2 (MeV)

Fig 7

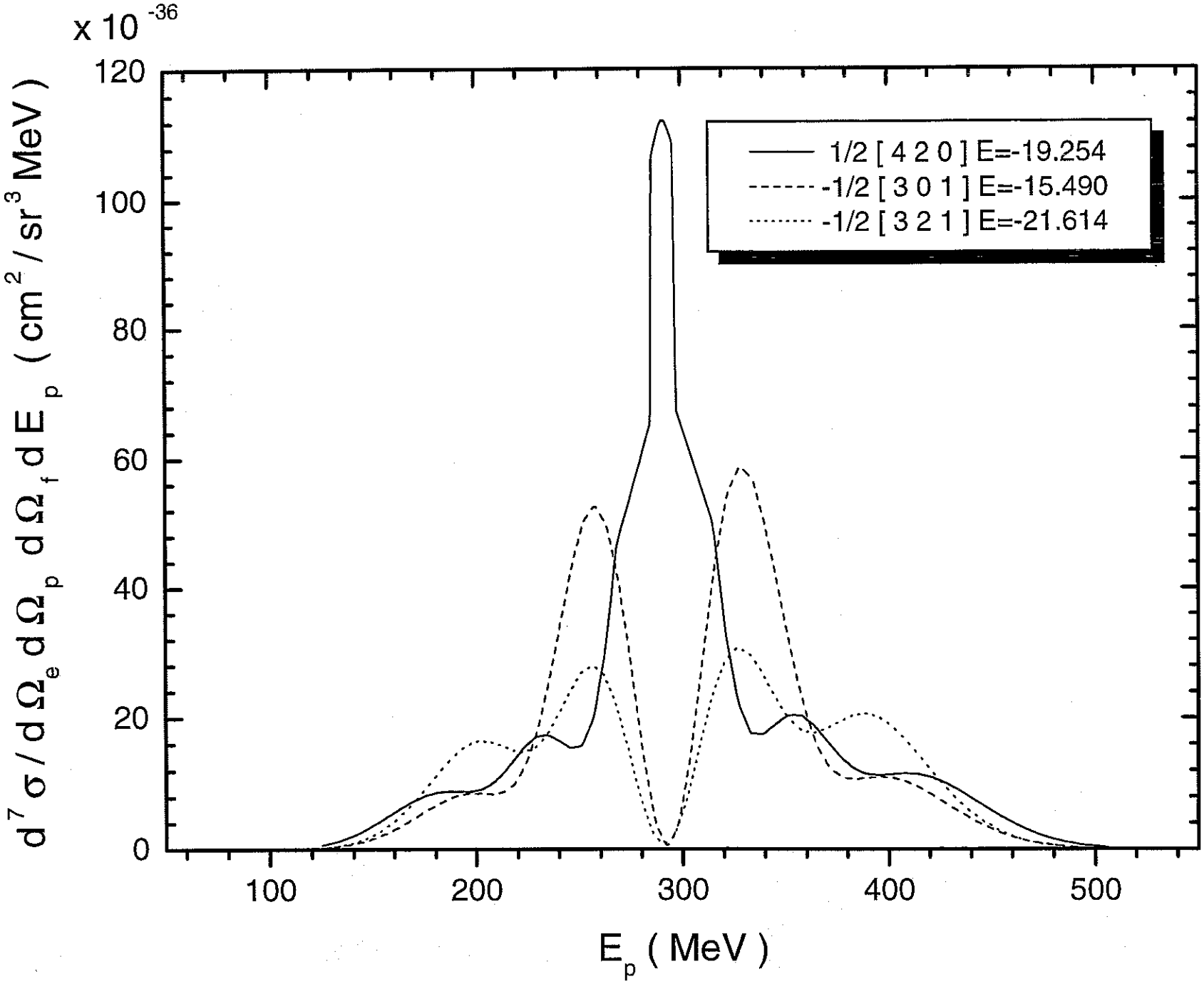
x 10 -36
120
100
80
60
40
20
0
100
200
300
400
500
d7σ / dΩe dΩp dΩf dEp (cm2 / sr3 MeV)
Ep (MeV)
1/2 [4 2 0] E=-19.254
-1/2 [3 0 1] E=-15.490
-1/2 [3 2 1] E=-21.614

Fig 8

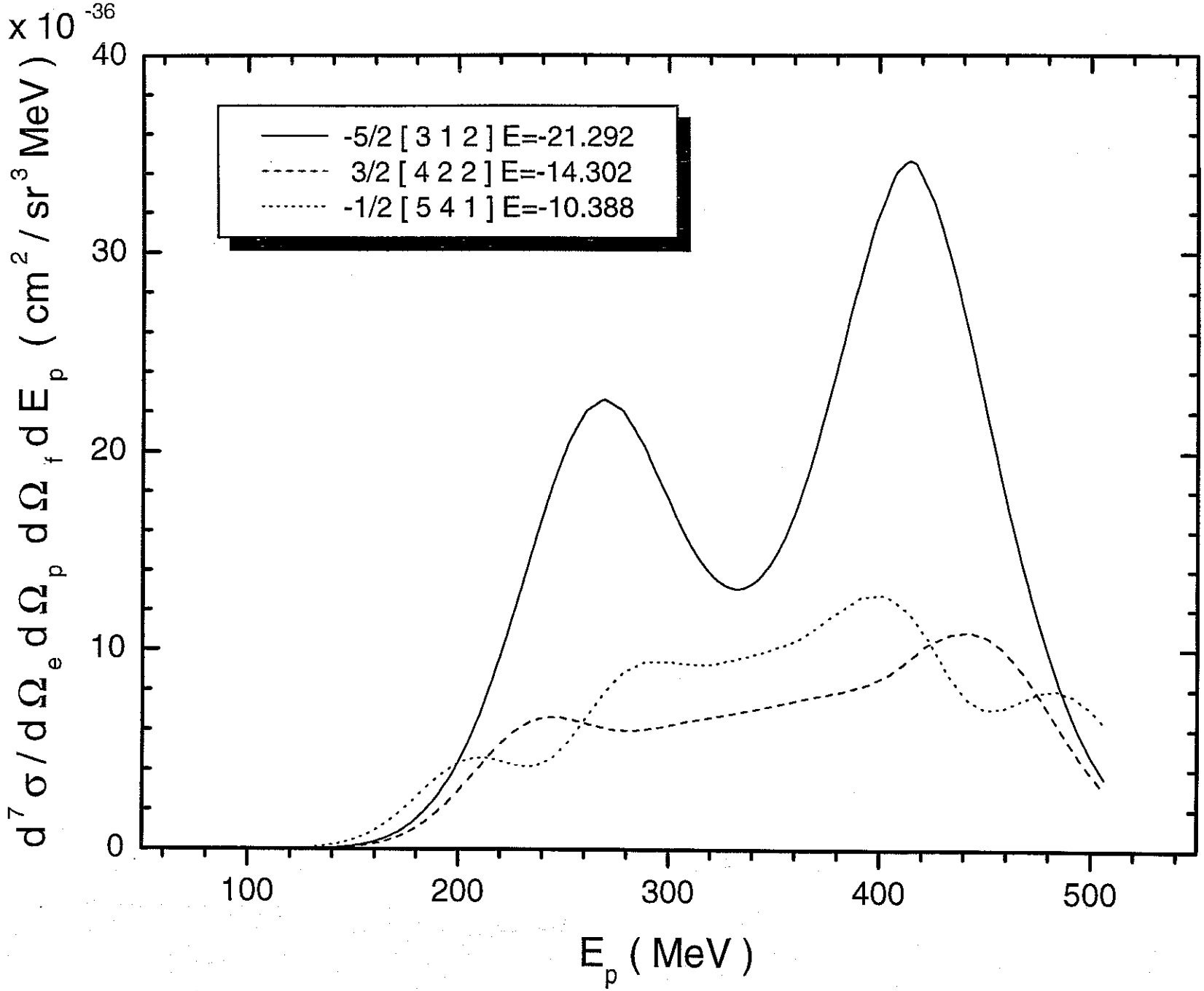
x 10 -36
d 7 σ / d Ω e d Ω p d Ω f d E p (cm 2 / sr 3 MeV)
40
30
20
10
0
100
200
300
400
500
E p (MeV)
-5/2 [3 1 2] E=-21.292
3/2 [4 2 2] E=-14.302
-1/2 [5 4 1] E=-10.388

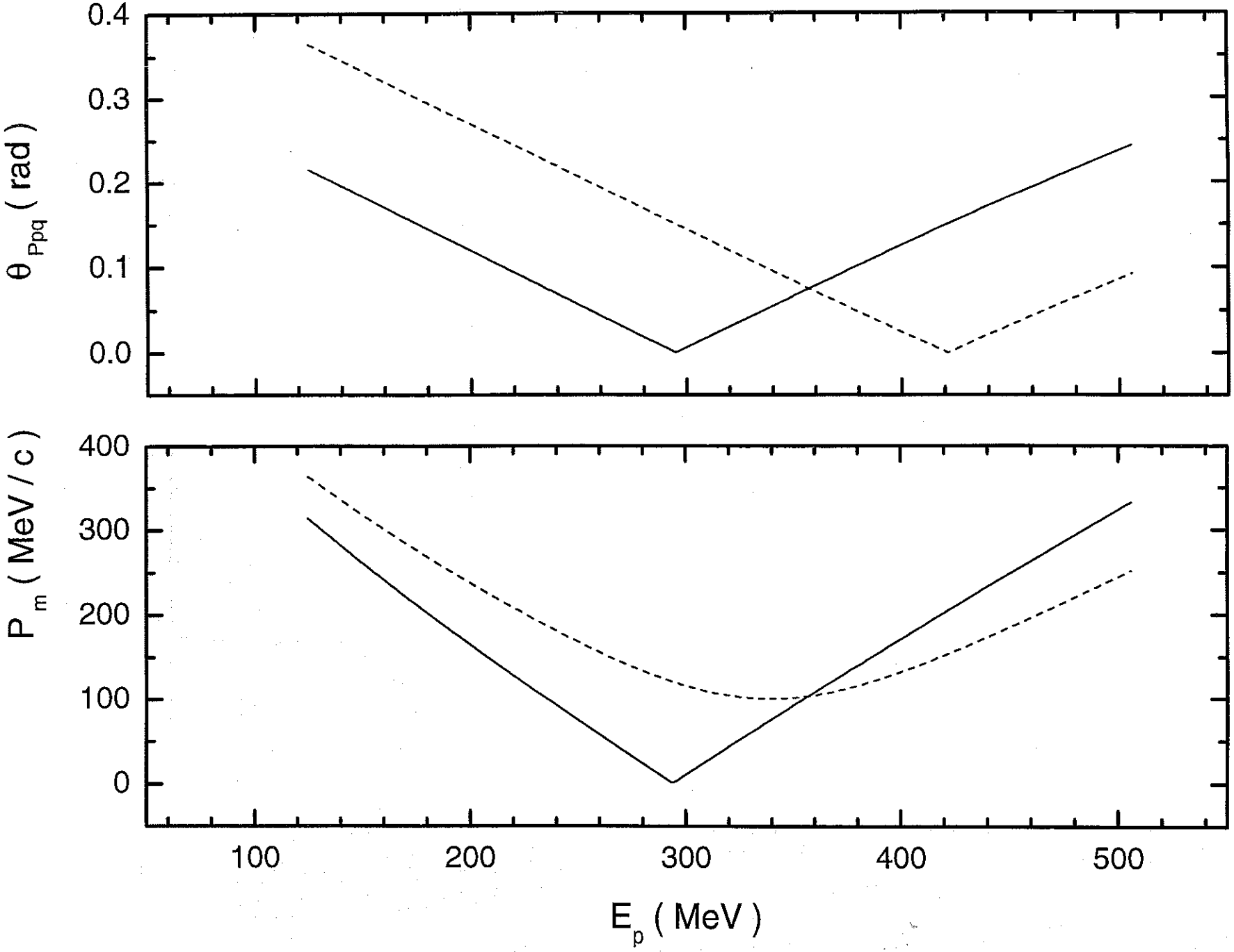
0.4
0.3
0.2
0.1
0.0
θ Ppq (rad)
400
300
200
100
0
P m (MeV / c)
100
200
300
400
500
E p (MeV)